NJC

PAPER

View Article Online
View Journal | View Issue

Cite this: *New J. Chem.*, 2015, 39, 9918

Selective construction of junctions on different facets of $BiVO_4$ for enhancing photo-activity

Peng Wang,[ab] Jin You Zheng,[a] Dun Zhang[b] and Young Soo Kang*[a]

Received (in Montpellier, France) 14th July 2015,
Accepted 13th October 2015

DOI: 10.1039/c5nj01836f

www.rsc.org/njc

A novel ternary $Ag/BiVO_4/Co_3O_4$ hybrid photocatalyst was designed by constructing a metal–semiconductor junction and a p–n junction on electron-rich {010} facets and hole-rich {110} facets of $BiVO_4$, respectively. The $Ag/BiVO_4/Co_3O_4$ hybrid photocatalyst exhibits enhanced photocatalytic activity for rhodamine B degradation, which is over 8 times that of bare $BiVO_4$ under simulated solar light. It was proven that the combination of a metal–semiconductor junction and a p–n junction further promotes the charge transferring across the interface, and results in an additional effect of two single junctions for improving photo-activity. This research provides a deep insight about the co-working mechanism between the two heterojunctions, and it will propose a new concept for designing a highly efficient photo-catalyst system.

1. Introduction

Water purification is quite important for human health.[1–3] Over recent decades, numerous effective methods have been widely used for water purification, including chlorination, ozonization, UV radiation and so forth.[4–7] However, these treatments have some disadvantages, such as the production of toxic by-products, transport and storage of chemicals as well as high energy needs.[7] Photocatalysis has been proven to be a promising process for water purification due to its advantages such as non-selective, and no need of additional chemicals.[8–11]

Bismuth vanadate ($BiVO_4$) has received much attention among the visible light-active photo-catalysts.[12–14] $BiVO_4$ has three main crystal structures, tetragonal zircon, tetragonal scheelite and monoclinic scheelite. The monoclinic scheelite phase of $BiVO_4$ has a band gap of 2.4 eV and has been demonstrated to exhibit much higher photo-catalytic activity in visible light than the other two phases.[15] However, the photo-activity of $BiVO_4$ alone is not very impressive because of the relatively fast recombination of photogenerated electron–hole pairs.[16]

Designing and constructing heterojunctions, such as p–n junctions, metal–semiconductor (m–s) junctions and so forth, is an effective way to improve the electron–hole separation.[17] Many researchers have reported the advantages of heterojunctions in enhancing the activity of a photocatalyst.[17–20] Recently, multi-junction photocatalyst systems were designed to further improve photocatalytic activity, such as $Ag/Ag_3PO_4/BiPO_4$ (ref. 21) and $Cu–TiO_2–Cu_2O$[22] hybrid catalysts. In the present research, the band position and the Fermi level were firstly taken into consideration for selecting interfacial junction materials, since the matching of band energy between two components is one of the most important conditions for designing efficient junctions.[17] Actually, the distribution of holes and electrons over the semi-conductor surface under irradiation is an essential factor that should be considered for selecting the construction location of junctions. However, junctions were usually constructed over the semi-conductor surface randomly without considering the location in the present research. In this case, the construction of junctions can hardly achieve optimal hole–electron separation efficiency, and it is also hard to anticipate the co-working mechanism between different junctions for electron–hole separation.

Recently, it was reported that photo-generated electrons and holes can be spatially separated onto different facets of $BiVO_4$.[23] Accordingly, we can selectively construct suitable junctions on different facets of $BiVO_4$ for improving photoactivity based on the charge separation among different facets. The semiconductor p–n junction is an effective architecture for the highly efficient charge collection and separation. $BiVO_4$ is an n-type semiconductor, so it is reasonable to design p–n junctions on hole-rich facets of $BiVO_4$ to facilitate the transfer of holes to the p-type semiconductor, and thus avoid the recombination of holes with electrons in $BiVO_4$. To deposit noble metal nanoparticles on the surface of the semiconductor is another effective method to create a space-charge separation region. These metal nanoparticles can act as a sink for photo-induced electrons, thereby facilitating the charge separation and enhancing the photocatalytic activity. For their high activity as the sink for photo-induced electrons, a metal–semiconductor (m–s) junction

[a] *Korea Center for Artificial Photosynthesis and Department of Chemistry, Sogang University, Seoul 121-742, Korea. E-mail: yskang@sogang.ac.kr*
[b] *Key Laboratory of Marine Environmental Corrosion and Bio-fouling, Institute of Oceanology, Chinese Academy of Sciences, 7 Naihai Road, Qingdao 266071, China*

can be constructed over electron-rich facets of $BiVO_4$ to improve its photoactivity. So far, various noble metals such as platinum, aurum, and silver have been deposited on semiconductors to improve the photoactivity. Among them, silver is an attractive one because of its low cost and as well as its effective electron trapping ability.[24]

In this research, silver and cobalt oxide were selectively deposited onto electron-rich facets and hole-rich facets of $BiVO_4$ crystals, thereby constructing the metal–semiconductor junction and the p–n junction over $BiVO_4$. Rhodamine B degradation was utilized as a probe to evaluate the photo-activity of as-fabricated photocatalysts. It was demonstrated that the photoactivity of $BiVO_4$ with the metal–semiconductor junction and the p–n junction selectively constructed on {010} and {110} facets of $BiVO_4$ crystals was dramatically enhanced compared with the pure $BiVO_4$, and the combination of the two junctions results in the additional effect of two single junctions for improving photo-activity. This work will give a deep insight to understand the co-working mechanism of multi-junctions in a hybrid photocatalyst system, and it will provide a general concept for constructing highly effective photocatalysts.

2. Experimental section

2.1 Synthesis of photocatalysts

2.1.1 Synthesis of $BiVO_4$. A $BiVO_4$ crystal sample was synthesized by a hydrothermal method. In a typical procedure, the precursors $Bi(NO_3)_3{\cdot}5H_2O$ (50 mmol) and NH_4VO_3 (50 mmol) were dissolved in 10 mL of 4.0 M HNO_3 solution and 10 mL 2.0 M NaOH solution, respectively. These two solutions were mixed slowly to form a yellowish suspension, and the pH value of the solution was then adjusted to be 1.0 with sodium hydroxide under stirring. After stirring for 0.5 h, the suspension was transferred into a Teflon-lined stainless steel autoclave with a capacity of 25 mL, and reacted at 150 °C for 12 h. After hydrothermal reaction, the precipitate was washed and centrifuged in de-ionized water three times, and finally dried overnight at 60 °C.

2.1.2 Facet-selective photo-deposition of silver and/or cobalt oxide. For the facet-selective photo-deposition on $BiVO_4$, similar procedures were performed for single silver reductive-deposition, single cobalt oxide oxidative-deposition, and simultaneous silver reductive-deposition and cobalt oxide oxidative-deposition. Typically, 0.1 g of $BiVO_4$ powder was dispersed into 50 mL of aqueous solution with a calculated amount of metal precursors upon stirring. Photo-deposition was performed for 4 h at room temperature, using a 300 W Xe lamp (Max-302, Asahi Spectra, Japan) as a light source. After photo-deposition, the $BiVO_4$ sample was filtered, repeatedly washed with de-ionized water, and finally dried at 40 °C in a vacuum oven for 12 h. For single silver reductive-deposition, a 2 g L^{-1} $AgNO_3$ solution with a volume of 50 mL was used as the precursor solution, and the as-obtained sample after photo-deposition was denoted as $BiVO_4$–Ag. The single cobalt oxide oxidative-deposition was performed in a 50 mL solution mixed with 1.456 g L^{-1} $Co(NO_3)_2$ and 4 g L^{-1} $NaIO_3$, in which, $Co(NO_3)_2$ was used as a precursor, and $NaIO_3$ was used as an electron acceptor. The as-obtained sample after single oxidative-deposition was denoted as $BiVO_4$–Co_3O_4. The simultaneous silver reductive-deposition and cobalt oxide oxidative-deposition was performed by a two-step procedure. At first, the single cobalt oxide was deposited onto $BiVO_4$ in a mixed solution with 1.456 g L^{-1} $Co(NO_3)_2$ and 4 g L^{-1} $NaIO_3$. After 4 h of photo-deposition, the $BiVO_4$ sample was filtered, washed with de-ionized water, and then transferred into 2 g L^{-1} $AgNO_3$ solution. After photo-deposition of Ag, the $BiVO_4$ sample was filtered, repeatedly washed with de-ionized water, and finally dried at 40 °C in a vacuum oven for 12 h. The as-obtained sample after two-step deposition was denoted as $BiVO_4$–Ag/Co_3O_4.

2.2 Characterization

X-ray diffraction (XRD, Rigaku miniFlex-II desktop X-ray diffractometer, Cu-Kα radiation with λ = 0.154056 nm) was used to determine crystallinity and the crystal structure of the as-fabricated $BiVO_4$ samples. The morphologies of the samples were observed using a scanning electron microscope (SEM, Hitachi Horiba S-4300) operated at 20 kV, and using a transmission electron microscope (TEM, JEOL. JEM-2010). The chemical states of Ag and Co on $BiVO_4$ were determined using an X-ray photoelectron spectroscopy apparatus (PHI Quantera SXM). The energies of all spectra were shifted by correcting the C 1s peak to 284.6 eV for energy calibration. The room temperature photoluminescence (PL) of the powder samples was measured using a Hitachi F-7000 fluorescence spectrophotometer, using the 325 nm excitation of a Xenon lamp.

2.3 Dye photodegradation experiment

The photocatalytic efficiencies of all the prepared catalysts were evaluated by photodegrading rhodamine B (RhB) under simulated sunlight irradiation, which was sourced using a 300-W Xe lamp. In the degradation experiment, 100 mg of photocatalyst was suspended in 50 mL of aqueous solution with 10 mg L^{-1} RhB. Before irradiation, the RhB solution with a photocatalyst was stirred in the dark for 30 min to reach an adsorption/desorption equilibrium between RhB and the photocatalyst. During irradiation, approximately 3 mL of suspensions were collected at given time intervals and centrifuged to remove the photocatalyst particles. After that, the absorption spectra of the remaining sample solutions were recorded on the UV-vis equipment. Photocatalytic degradation over each sample was evaluated by the temporal concentration of RhB, which was determined in terms of their standard concentration *versus* absorbance curves and the changes in intensity of the absorbance at the corresponding absorption band maximum of RhB (554 nm).

3. Results and discussion

3.1 Morphology and composition characterization

X-ray diffraction was used to determine crystallinity and the crystal structure of the as-fabricated $BiVO_4$ samples. According to the X-ray diffraction patterns of as-prepared $BiVO_4$ powder

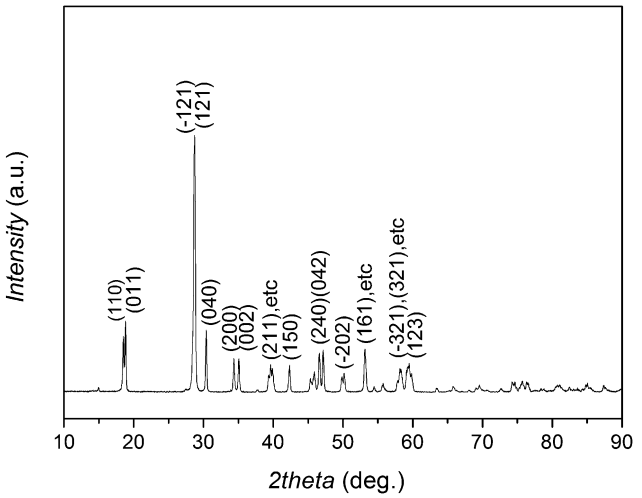

Fig. 1 X-ray diffraction pattern of as-prepared monoclinic sheelite $BiVO_4$ powder.

(Fig. 1), it is indicated that the as-prepared $BiVO_4$ is a monoclinic scheelite according to the standard JCPDS card no. 14-0688.

Fig. 2 shows the morphologies of bare $BiVO_4$ powder and $BiVO_4$ powder deposited with Ag and Co_3O_4 particles. It can be observed that the exposed facets of $BiVO_4$ are mainly composed of two facets, which are denoted as {010} and {110} facets, respectively (Fig. 2a). After photo-reduction deposition in silver nitrate aqueous solution, Ag particles with diameters of around tens of nanometers were selectively deposited on the electron-rich {010} facets of $BiVO_4$ (Fig. 2b). XPS was utilized to confirm the oxidation state of these Ag particles on $BiVO_4$. From Fig. 4a, Ag 3d peaks can be easily observed from the survey spectrum of sample $BiVO_4$–Ag. The high revolution of the Ag 3d spectrum (Fig. 4b) shows that two peaks appeared at 368.2 and 374.2 eV are well corresponded with Ag $3d_{5/2}$ and Ag $3d_{3/2}$ binding energies, respectively. The splitting of the 3d doublet is 6.1 eV, indicating the metallic nature of silver.[25] Thus, it is proven that the photo-generated electrons are spatially separated onto the {010} facets of $BiVO_4$ under irradiation, and they are readily available for the reduction reaction of silver ions. It is expected that the photo-reduction of silver ions (eqn (1)) on {010} facets of $BiVO_4$ is accompanied by the elimination of photo-generated holes on {110} facets by water oxidation (eqn (2)), which can be expressed as follows:

$$Ag^+ + e^- \rightarrow Ag \quad (1)$$

$$2H_2O + 4h^+ \rightarrow O_2 + 4H^+ \quad (2)$$

Fig. 2c and d show the morphologies of $BiVO_4$ powder after deposition of Co_3O_4 particles by the photo-oxidization deposition method in aqueous solution mixed with $Co(NO_3)_2$ and $NaIO_3$. As we expect, Co_3O_4 particles are selectively deposited on the {110} facets of $BiVO_4$. TEM images (Fig. 3a and b) confirm that the Co_3O_4 particle layer with a thickness of about 20 nm was formed on the {110} facets of $BiVO_4$ after photo-oxidization deposition. Fig. 3c shows the compositional scan profile (a blue line marked in the TEM image in Fig. 3b) of the sample $BiVO_4$–Co_3O_4. It clearly shows a strong Co signal at the edge of powder, further proving the selective deposition of Co species on {110} facets of $BiVO_4$. The high revolution of the Co 2p XPS spectrum of sample $BiVO_4$–Co_3O_4 shows a doublet containing a low energy band (Co $2p_{3/2}$) and a high energy band

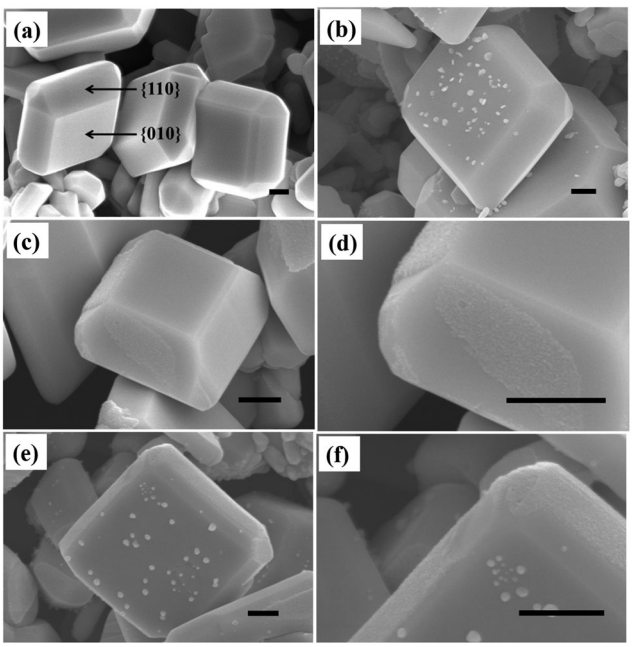

Fig. 2 Morphologies of as-prepared $BiVO_4$ powder (a), sample $BiVO_4$–Ag (b), sample $BiVO_4$–Co_3O_4 (c and d) and sample $BiVO_4$–Ag/Co_3O_4 (e and f). Scale bar = 500 nm.

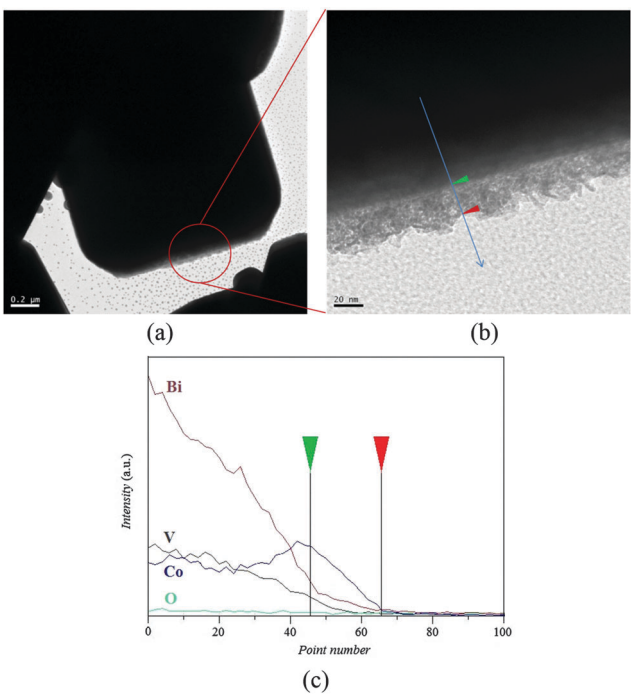

Fig. 3 TEM images of sample $BiVO_4$–Co_3O_4 (a and b), and the EDS line scan of Bi, V, Co and O elements on sample $BiVO_4$–Co_3O_4 along the blue line marked in (b) and (c).

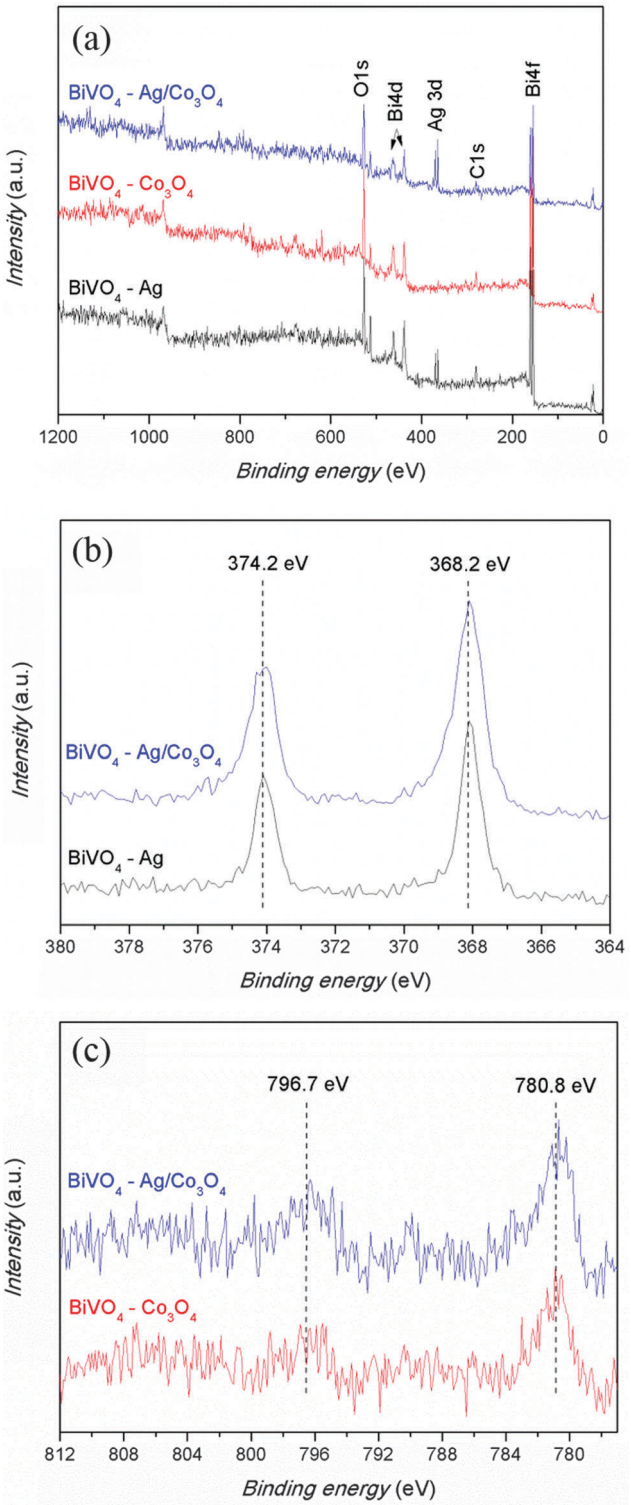

Fig. 4 XPS spectra of three kinds of photo-catalysts ($BiVO_4$–Ag, $BiVO_4$–Co_3O_4 and $BiVO_4$–Ag/Co_3O_4): (a) survey spectra, and high resolution of (b) Ag 3d and (c) Co 2p spectra.

($Co\ 2p_{1/2}$) at 780.8 and 796.7 eV (Fig. 4c), respectively, indicating that the deposited cobalt species can be ascribed to Co_3O_4.[26] Accordingly, it is expected that Co^{2+} ions are oxidized into Co_3O_4 on the {110} facets of $BiVO_4$ crystals with the assistance of using IO_3^- as sacrificial electron acceptors. The reactions can be described as eqn (3) and (4):

$$3Co^{2+} + 4H_2O + 2h^+ \rightarrow Co_3O_4 + 8H^+ \quad (3)$$

$$2IO_3^- + 10e^- + 12H^+ \rightarrow I_2 + 6H_2O \quad (4)$$

After the selective photo-deposition of Ag and Co_3O_4 particles on $BiVO_4$, we further investigated the photo-deposition of dual components (Ag and Co_3O_4) using a two-step procedure including photo-oxidation deposition and the following photo-reduction deposition. Using this method, Ag and Co_3O_4 particles were deposited separately on the {010} and {110} facets of $BiVO_4$ powder, respectively (Fig. 2e and f). XPS was utilized to check the oxidation state of silver and cobalt on $BiVO_4$ crystals after dual component deposition. It was observed that two typical Ag 3d peaks ($Ag\ 3d_{5/2}$ and $Ag\ 3d_{3/2}$) of $BiVO_4$–Ag/Co_3O_4 are located at the same position with that of the $BiVO_4$–Ag sample (Fig. 4b), and the two typical Co 2p peaks ($Co\ 2p_{1/2}$ and $Co\ 2p_{3/2}$) of the $BiVO_4$–Ag/Co_3O_4 sample are also located at the same position with that of the $BiVO_4$–Co_3O_4 sample (Fig. 4c). It was demonstrated that the selective deposition of Ag and Co_3O_4 on two facets was successfully accomplished by the two-step photo-deposition procedure. Thus, the p–n junction and the m–s junction can be selectively constructed on hole and electron rich facets of $BiVO_4$. XPS is generally utilized to determine the content of single composition in the composite material. According to the XPS result in Fig. 4, the content of Ag and Co_3O_4 loaded over BiVO4 can be calculated to be 2.026 wt% and 0.137 wt%, respectively.

3.2 Optical absorption properties

Diffuse reflectance spectroscopy is an appropriate tool to depict the energy band structure feature of a semiconductor, which is relevant to the optical absorption properties considered as a pivotal factor in determining its photocatalytic activity. Fig. 5a shows the UV-vis diffuse reflectance spectra of the four kinds of $BiVO_4$ samples ($BiVO_4$, $BiVO_4$–Ag, $BiVO_4$–Co_3O_4, and $BiVO_4$–Ag/Co_3O_4). The pure $BiVO_4$ sample presents intense absorption in the visible region until ~525 nm in addition to that in the UV light region.[27,28] For the monoclinic scheelite $BiVO_4$, the visible absorption band is designated to the transition from a valence band formed by Bi 6s or a hybrid orbital of Bi 6s and O 2p to a conduction band of V 3d.[28] The band gap (E_g) of the sample can be estimated according to formula $ah\nu = A(h\nu - E_g)^n$,[28] where a, h, ν, A and E_g are the absorption coefficient, Planck's constant, the incident light frequency, a constant and the band gap energy, respectively. For $BiVO_4$, the value of n is 1/2, which indicates that $BiVO_4$ is a direct band gap material. From the plots of $(ah\nu)^2$ *versus* photon energy ($h\nu$) shown in Fig. 5b, the band gap energy of $BiVO_4$ could be estimated to be 2.43 eV.[29]

After the deposition of Co_3O_4, the ability of light absorption is enhanced greatly. In accordance with that, the color of the sample changed from yellow of pure $BiVO_4$ to grey-yellow of $BiVO_4$–Co_3O_4 (Fig. 5c). This should be attributed to the broad absorption at 500–900 nm characteristic of the Co_3O_4 phase.[30] After the deposition of Ag, the absorbance edge of $BiVO_4$–Ag shows a slight red shift, and the absorption of $BiVO_4$ in the

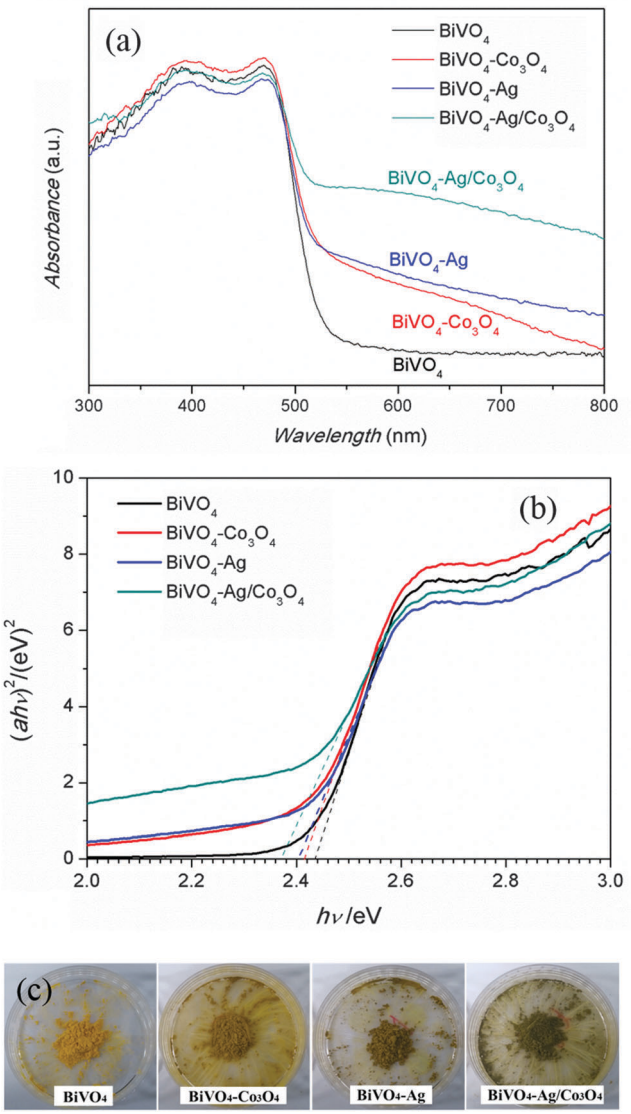

Fig. 5 UV-VIS DRS of samples $BiVO_4$, $BiVO_4$–Ag, $BiVO_4$–Co_3O_4, and $BiVO_4$–Ag/Co_3O_4 (a), plots of $(\alpha h\nu)^2$ *vs.* $h\nu$ (b), and photos of samples $BiVO_4$, $BiVO_4$–Ag, $BiVO_4$–Co_3O_4, and $BiVO_4$–Ag/Co_3O_4 (c).

range of 500–800 nm is intensified, both of it can be attributed to the surface plasmon resonance effect of silver nanoparticles.[31] After the deposition of two components (Ag and Co_3O_4), the absorption of $BiVO_4$ in the range of 500–800 nm is further enhanced in comparison with $BiVO_4$ samples deposited with a single Ag or single Co_3O_4 component, and this result agrees with the phenomenon that the color of sample $BiVO_4$–Ag/Co_3O_4 is darker than samples $BiVO_4$–Ag and $BiVO_4$–Co_3O_4. It must be emphasized that the photocatalytic activity can be greatly increased when the band gap is narrowed, which can facilitate the generation of electrons and holes and the excitation of an electron from the valence band to the conduction band.[32] The estimated E_g of as-fabricated $BiVO_4$–Co_3O_4, $BiVO_4$–Ag and $BiVO_4$–Ag/Co_3O_4 from the intercept of the slopes to the plots were 2.41, 2.40 eV and 2.37 eV, respectively. The band gaps of these samples decreased compared to pure $BiVO_4$ (2.43 eV), and the lower band gap implies a higher photocatalytic activity under visible light under irradiation in the presence of Ag and Co_3O_4.

3.3 Photocatalytic activity and the mechanism

To prove the contribution of Ag and Co_3O_4 to the photocatalytic activities of $BiVO_4$, and to understand the co-working mechanism of a multi-junction in a hybrid photocatalyst system, the photocatalytic activities of samples $BiVO_4$, $BiVO_4$–Ag, $BiVO_4$–Co_3O_4, and $BiVO_4$–Ag/Co_3O_4 were firstly measured in the liquid phase reaction under the simulated solar light irradiation. The decomposition of RhB in the aqueous solution was chosen as the photoreaction probe. As shown in Fig. 6, the adsorption of RhB over all samples in dark condition could be neglected. After 120 min of the simulated solar light irradiation, the degradation extent of RhB dye with the assistance of pure $BiVO_4$ can only reach around 10%, indicating that $BiVO_4$ only achieves low activity for degradation of RhB. In the presence of $BiVO_4$ powders deposited with a single component (Ag or Co_3O_4),

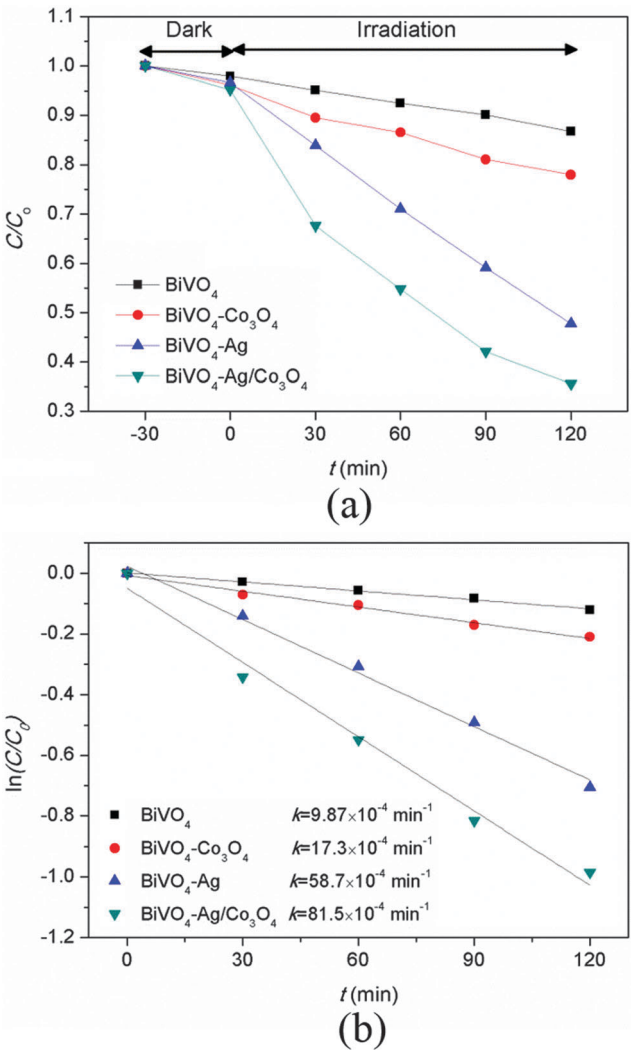

Fig. 6 Photo-degradation extent of RhB dye *versus* irradiation time in the presence of samples $BiVO_4$, $BiVO_4$–Co_3O_4, $BiVO_4$–Ag, $BiVO_4$–Ag/Co_3O_4 (a), and kinetic curves of the photo-degradation of RhB dye under irradiation (b).

the degradation extents of RhB dye increase to 20% (sample $BiVO_4$–Co_3O_4) and 52% (sample $BiVO_4$–Ag), respectively. It indicates that the single Ag or Co_3O_4 component on $BiVO_4$ powder can increase photocatalytic activities. In the presence of sample $BiVO_4$–Ag/Co_3O_4, the degradation extent of RhB is further increased to 65%, proving that a better performance can be achieved by depositing the two components simultaneously.

If the photo-degradation of RhB is considered as a pseudo-first-order reaction, its photocatalytic reaction kinetics can be expressed as follows: $\ln(C/C_0) = -kt$, where C is the concentration of the RhB at time t, C_0 is the initial concentration of the RhB solution, and the slope k is the apparent reaction rate constant. Fig. 6b represents the photodegradation curves of RhB in the form of $\ln(C_0/C)$ as a function of irradiation time. It can be found that the apparent reaction rate constant of sample $BiVO_4$ for RhB photo-degradation is 9.87×10^{-4} min^{-1}. After depositing the two components (Ag and Co_3O_4) simultaneously, the apparent reaction rate constant of sample $BiVO_4$–Ag/Co_3O_4 for RhB photo-degradation increases to 81.5×10^{-4} min^{-1}, which is almost ten times that of bare $BiVO_4$. It is proven that the deposition of the two components can significantly improve the photoactivity of the photocatalyst. It should be noticed that the apparent reaction rate constant of sample $BiVO_4$–Ag/Co_3O_4 is almost equal to the sum of that of samples $BiVO_4$–Ag and $BiVO_4$–Co_3O_4 ($k_{BiVO_4-Ag/Co_3O_4} \approx k_{BiVO_4-Ag} + k_{BiVO_4-Co_3O_4}$), indicating that there is no synergetic effect between the p–n junction and the metal–semiconductor junction in the Co_3O_4/$BiVO_4$/Ag system.

PL emission spectra are often used to examine the efficiency of charge carrier trapping, immigration and transfer, as well as to understand the fate of electron/hole pairs in semiconductor particles. Fig. 7 shows the room temperature PL emission spectra of samples $BiVO_4$, $BiVO_4$–Co_3O_4, $BiVO_4$–Ag, and $BiVO_4$–Ag/Co_3O_4. The PL peak of as-fabricated $BiVO_4$ powder was observed at around 540 nm, and it corresponds to the recombination of the hole formed in the O 2p band and the electron in the V 3d band. In comparison with bare $BiVO_4$, the PL peak is reduced after depositing a single Co_3O_4 or single Ag component, indicating that the existence of the single component can help to reduce the recombination of electrons and holes. The PL peak of the sample $BiVO_4$–Ag/Co_3O_4 is further reduced after depositing Ag and Co_3O_4 simultaneously. This result indicates that the recombination of photogenerated charge carriers is greatly inhibited, and photo-activity of the phocatalyst will be enhanced greatly after depositing Ag and Co_3O_4 simultaneously.

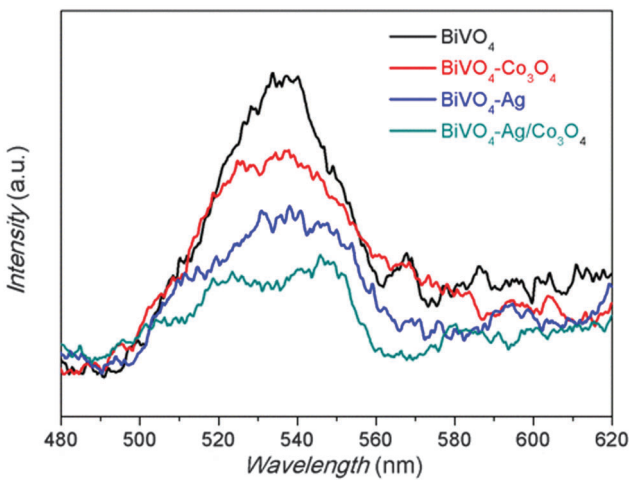

Fig. 7 Room temperature PL emission spectra of samples $BiVO_4$, $BiVO_4$–Co_3O_4, $BiVO_4$–Ag, and $BiVO_4$–Ag/Co_3O_4.

Based on these results, the charge separation process of Ag/$BiVO_4$/Co_3O_4 heterogeneous structures can be proposed as Fig. 8. The band gap of $BiVO_4$ was evaluated to be 2.43 eV from the UV-vis spectrum. Therefore we presume the corresponding conduction band (E_{CB}) and valence band (E_{VB}) positions of $BiVO_4$ at the point of zero charge through the following equations:[33]

$$E_{CB} = x - E_0 - \frac{1}{2}E_g \quad (5)$$

$$x = \frac{1}{2}(A_f + I_1) \quad (6)$$

where x is the bulk electronegativity of the compound, A_f and I_1 are the atomic electron affinity and the first ionization potential, respectively. E_0 is the energy of free electrons on the hydrogen scale (about 4.5 eV), and E_g is the band gap energy of the semiconductor. The position of the valence band edge can be determined by the equation of $E_{VB} = E_{CB} + E_g$. The calculation result shows that the bottom of the conduction band of $BiVO_4$ is around 0.32 eV *versus* the normal hydrogen electrode (NHE), while the top of the valence band is around 2.75 eV. Generally speaking, the conduction band potential of an n-type semiconductor is more negative (*ca.* 0.1–0.2 V) than the flat-band potentials,[33] so the Fermi level of metallic Ag (E_f = 0.69 V *vs.* NHE) is much lower than that of BiVO4.[34] On the {010} facet of $BiVO_4$, when Ag and $BiVO_4$ are in contact, electrons in $BiVO_4$ will transfer to the Ag particles to equilibrate the Fermi levels, and a Schottky barrier forms between Ag and $BiVO_4$. Furthermore, it was widely reported that Co_3O_4 is a kind of p-type semi-conductor with a conduction band edge and a valence band edge of Co_3O_4 of 0.37 eV and 2.44 eV *vs.* NHE. Before contact of p-type Co_3O_4 with n-type $BiVO_4$, the conduction band edge of p-type Co_3O_4 is lower than that of n-type $BiVO_4$, and the Fermi level of Co_3O_4 is also lower than that of $BiVO_4$, as shown in Fig. 8a. After the p-type Co_3O_4 nanoparticles are tightly assembled on the hole-rich facet {110} of n-type $BiVO_4$ nanocrystals, the Fermi level of Co_3O_4 is increased up, while the Fermi level of $BiVO_4$ is lowered until an equilibrium state is formed as shown in Fig. 8b. Meanwhile, with increasing and/or lowering the Fermi level, the whole energy band of Co_3O_4 is increased while that of $BiVO_4$ is lowered, and as a result, the conduction band edge of p-type Co_3O_4 is higher than that of n-type $BiVO_4$, leading to the formation of a p–n junction at the interface between Co_3O_4 and $BiVO_4$ crystals.

In the Ag/$BiVO_4$/Co_3O_4 system, the electrons and holes transfer separately to {010} and {110} facets of $BiVO_4$ for the potential difference between the two facets under irradiation. On the electron-rich {010} facet, electrons can be easily injected

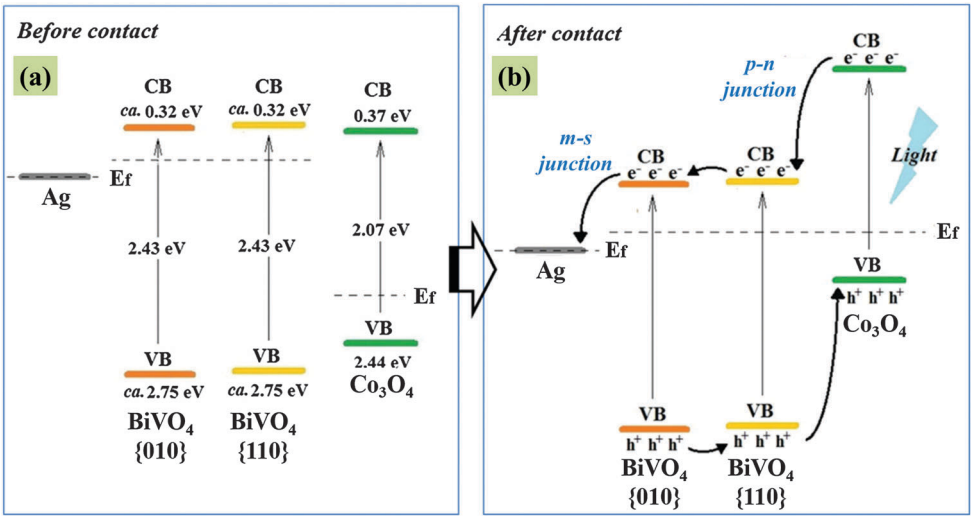

Fig. 8 A schematic on the charge transfer processes of the Ag/$BiVO_4$/Co_3O_4 hybrid photocatalyst.

into the Fermi level of Ag. The metallic silver nanoparticles functioned as an electron sink to accept the photo-generated electrons from the excited semiconductor, thereby facilitating dioxygen reduction.[35] On the hole-rich {110} facet, the photo-generated holes on the valence band of n-type $BiVO_4$ can be promptly migrated to the valence band of p-type Co_3O_4, and the photo-generated electrons on the conduction band of p-type Co_3O_4 can be transferred to the conduction band of n-type $BiVO_4$. Such a migration of photo-generated carriers can be promoted by the internally formed electric field. Therefore, the photo-generated electrons and holes of n-type $BiVO_4$ can be separated effectively by the p–n junctions formed between the p-type Co_3O_4 and the n-type $BiVO_4$ interface, and the recombination of electron–hole pairs can be substantially reduced. As a result, Ag/$BiVO_4$/Co_3O_4 had a quicker charge separation and a slower charge recombination process than the single or two component catalyst system. The combination of the two junctions in the Ag/$BiVO_4$/Co_3O_4 system results in additional effect for improving photo-activity.

4. Conclusion

A novel ternary Ag/$BiVO_4$/Co_3O_4 hybrid photocatalyst was designed by the photo-deposition method. In this hybrid photocatalyst, a metal–semiconductor junction and a p–n junction were separately constructed over {010} facets and {110} facets of $BiVO_4$, which are electron-rich and hole-rich facets, respectively. The Ag/$BiVO_4$/Co_3O_4 system exhibits enhanced photocatalytic activity for rhodamine B degradation, which is over 8 times that of bare $BiVO_4$ under irradiation. The apparent reaction rate constant of sample $BiVO_4$–Ag/Co_3O_4 is almost equal to the sum of that of samples $BiVO_4$–Ag and $BiVO_4$–Co_3O_4. It is proven that the combination of the two junctions further promotes the charge transferring across the interface, and results in an additional effect of the two single junctions for improving photo-activity. This research provides a deep insight about the co-working mechanism between two heterojunctions, and it will propose a new concept for designing a highly efficient photocatalyst system.

Acknowledgements

This research was supported by the Young Scientist Exchange Program between The Republic of Korea and the People's Republic of China, and The National Natural Science Foundation of China (No. 41476068).

References

1 J. M. C. Robertson, P. K. J. Robertson and L. A. Lawton, *J. Photochem. Photobiol., A*, 2005, **175**, 51–56.
2 H. A. Foster, I. B. Ditta, S. Varghese and A. Steele, *Appl. Microbiol. Biotechnol.*, 2011, **90**, 1847–1868.
3 X. Wang, X. Hu, H. Wang and C. Hu, *Water Res.*, 2012, **46**, 1225–1232.
4 J. Oh, D. E. Salcedo, C. A. Medriano and S. Kim, *J. Environ. Sci.*, 2014, **26**, 1238–1242.
5 Y. Mao, X. Wang, H. Yang, H. Wang and Y. F. Xie, *Chemosphere*, 2014, **117**, 515–520.
6 C. Poepping, S. E. Beck, H. Wright and K. G. Linden, *Water Res.*, 2014, **56**, 181–189.
7 E. Ortega-Gómez, P. Fernández-Ibáñez, M. M. Ballesteros Martín, M. I. Polo-López, B. Esteban García and J. A. Sánchez Pérez, *Water Res.*, 2012, **46**, 6154–6162.
8 T. Matsunaga, R. Tomoda, T. Nakajima and H. Wake, *FEMS Microbiol. Lett.*, 1985, **29**, 211–214.
9 P. Xiong and J. Hu, *Water Res.*, 2013, **47**, 4547–4555.
10 L. Zhang, H. Wang, Z. Chen, P. K. Wong and J. Liu, *Appl. Catal., B*, 2011, **106**, 1–13.
11 J. Cao, B. Luo, H. Lin and S. Chen, *J. Hazard. Mater.*, 2011, **190**, 700–706.
12 S. J. Hong, S. Lee, J. S. Jang and J. S. Lee, *Energy Environ. Sci.*, 2011, **4**, 1781–1787.

13 D. K. Zhong, S. Choi and D. R. Gamelin, *J. Am. Chem. Soc.*, 2011, **133**, 18370–18377.
14 R. Saito, Y. Miseki and K. Sayama, *Chem. Commun.*, 2012, **48**, 3833–3835.
15 H. Fan, T. Jiang, H. Li, D. Wang, L. Wang, J. Zhai, D. He, P. Wang and T. Xie, *J. Phys. Chem. C*, 2012, **116**, 2425–2430.
16 S. W. Cao, Z. Yin, J. Barber, F. Y. C. Boey, S. C. J. Loo and C. Xue, *ACS Appl. Mater. Interfaces*, 2012, **4**, 418–423.
17 H. Wang, L. Zhang, Z. Chen, J. Hu, S. Li, Z. Wang, J. Liu and X. Wang, *Chem. Soc. Rev.*, 2014, **435**, 234–5244.
18 W. Wang, X. Huang, S. Wu, Y. Zhou, L. Wang, H. Shi, Y. Liang and B. Zou, *Appl. Catal., B*, 2013, **134–135**, 293–301.
19 W. Wang, J. Wang, Z. Wang, X. Wei, L. Liu, Q. Ren, W. Gao, Y. Liang and H. Shi, *Dalton Trans.*, 2014, **43**, 6735–6743.
20 Z. He, Y. Shi, C. Gao, L. Wen, J. Chen and S. Song, *J. Phys. Chem. C*, 2014, **118**, 389–398.
21 Y. Lv, K. Huang, W. Zhang, B. Yang, F. Chi, S. Ran and X. Liu, *Ceram. Int.*, 2014, **40**, 8087–8092.
22 X. An, H. Liu, J. Qu, S. J. A. Moniz and J. Tang, *New J. Chem.*, 2015, **39**, 314–320.
23 R. Li, F. Zhang, D. Wang, J. Yang, M. Li, J. Zhu, X. Zhou, H. Han and C. Li, *Nat. Commun.*, 2013, **4**, 1432.
24 L. Chen, R. Huang, Y. J. Ma, S. L. Luo, C. T. Au and S. F. Yin, *RSC Adv.*, 2013, **3**, 24354–24361.
25 P. Zhang, C. Shao, Z. Zhang, M. Zhang, J. Mu, Z. Guo and Y. Liu, *Nanoscale*, 2011, **3**, 3357–3363.
26 J. Xu, P. Gao and T. S. Zhao, *Energy Environ. Sci.*, 2012, **5**, 5333–5339.
27 A. Kudo, I. Tsuji and H. Kato, *Chem. Commun.*, 2002, 1958.
28 Y. Lu, Y. S. Luo, H. M. Xiao and S. Y. Fu, *CrystEngComm*, 2014, **16**, 6059–6065.
29 Z. He, Y. Shi, C. Gao, L. Wen, J. Chen and S. Song, *J. Phys. Chem. C*, 2014, **118**, 389–398.
30 J. Wang and F. E. Osterloh, *J. Mater. Chem. A*, 2014, **2**, 9405–9411.
31 A. Y. Booshehri, S. C. K. Goh, J. Hong, R. Jiang and R. Xu, *J. Mater. Chem. A*, 2014, **2**, 6209–6217.
32 Z. Y. Bian, Y. Q. Zhu, J. X. Zhang, A. Z. Ding and H. Wang, *Chemosphere*, 2014, **117**, 527–531.
33 Y. Hu, D. Li, Y. Zheng, W. Chen, Y. He, Y. Shao, X. Fu and G. Xiao, *Appl. Catal., B*, 2011, **104**, 30–36.
34 W. Fan, S. Jewell, Y. She and M. K. H. Leung, *Phys. Chem. Chem. Phys.*, 2014, **16**, 676.
35 Y. Yang, J. Wen, J. Wei, R. Xiong, J. Shi and C. Pan, *ACS Appl. Mater. Interfaces*, 2013, **5**, 6201–6207.